ARTICLE

Check for updates

Conformation-Induced stiffening effect of crosslinked polymer thin films

Zhengyang Zhang [1], Pei Bai[1], Yuhan Xiao[1], Yunlong Guo [1,2✉] & Yanming Wang[1,2✉]

Nanoscale polymeric thin films are widely used in diverse modern applications, where a satisfactory mechanical performance is a requirement to their full functionality. The mechanical response of polymer films is strongly affected by the size effects under nano-confinement; however, the mechanism of such response in terms of molecular configurations and chain conformations has yet to be determined. In this work, we reveal the conformational origin of the stiffening behavior of crosslinked polymeric nanofilms via coarse-grained molecular dynamics and tailored experiments. We find that the biaxial modulus changes follow the alteration of polymer conformations, decoupled from size and thickness. We propose a theory to quantitatively link the elastic properties of the polymers to the distribution of their chain end-to-end distances, predicting a stiffening effect on uncoiled chains. Finally, we use such insight to obtain several PDMS nano-films of the same thickness but with a variability of two orders of magnitudes in their moduli.

[1] University of Michigan–Shanghai Jiao Tong University Joint Institute, Shanghai Jiao Tong University, 800 Dong Chuan Road, Minhang District, Shanghai 200240, China. [2] These authors jointly supervised this work: Yunlong Guo, Yanming Wang. ✉email: yunlong.guo@sjtu.edu.cn; yanming.wang@sjtu.edu.cn

Polymeric thin films are widely used in a broad range of applications including energy devices[1], transistors[2] and nanocomposites[3,4]. For instance, polymer semiconductors have their own advantages in wearable electronics, owing to their high flexibility, stretchability and crack resistance[5,6]. In nanofabrication, polymer films often act as nanoscale pattern generators by maintaining their topological pattern in prestressing and constrained shrinking[7]. In all these scenarios, the mechanical behaviors of polymer films are considered of vital importance to meet their functional requirements, especially when the thickness of the films is restricted to nanoscale. It has been reported that under nanoconfinement, the mechanical properties, such as elastic moduli of polymeric films, drastically change with decreasing film thickness[8–12]. To carefully examine these effects, tremendous experimental efforts have been made to measure mechanical responses at nanoscale by techniques such as nanoindentation[13–15], surface buckling[16], uniaxial tension[17], capillary wrinkling[18] and micro vibration[19], for both freestanding films and those in contact with substrates. However, to date, how the mechanical properties of a polymeric film are related to its intrinsic microstructure is still largely veiled in secrecy. For example, both positive[17,20–22] and negative[23,24] correlations between film thickness and mechanical behavior have been seen in different polymer systems. Though several factors, including interfacial mobility[25,26], substrate texture[17,19,27,28], and processing procedures[29], have been proposed to explain these correlations, the exact linkage between the change of material mechanical property and the alteration of its intrinsic microscopic properties has not been established. This is mainly hindered by the difficulty in direct observation of polymer chains, originated from the complex and random nature of their conformations. As an alternative approach, in recent years, computational techniques such as Monte Carlo simulations[30], classical molecular dynamics[31], and coarse-grained molecular dynamics[32–35], gradually become pivotal in predicting mechanical properties of polymer films, as an effective means to describe the microstructures of polymer network.

In this paper, we aim to trace the microscopic origin hidden behind the thickness-dependent elastic properties of crosslinked polymeric system, in aspects of their intrinsic conformations. Balancing between the computing efficiency and model accuracy, we develop a coarse-grained molecular dynamics (CGMD) framework containing carefully designed macro and micro descriptors to comprehensively investigate the elastic behaviors of the polymer system. Based on the results produced by the aforementioned framework, we propose a scaling law to link the biaxial modulus with the distribution of end-to-end distances, where conformation-induced stiffening effects are considered as an extension to the traditional entropic elasticity contribution. Finally, adopting model-guided processing protocols, we fabricate crosslinked PDMS films with different thicknesses, followed by elastic modulus measurements using an in-house micro vibration system. The results show that the PDMS films made from different fabrication pathways, though at approximately the same thickness, may exhibit up to a two-order-of-magnitude difference in moduli. This again suggests that the drastic change in elastic responses of polymeric systems is expected to originate from the conformational alterations, further than a nanoconfinement effect[15,35] or a surface tension induction[25] elaborated in literatures.
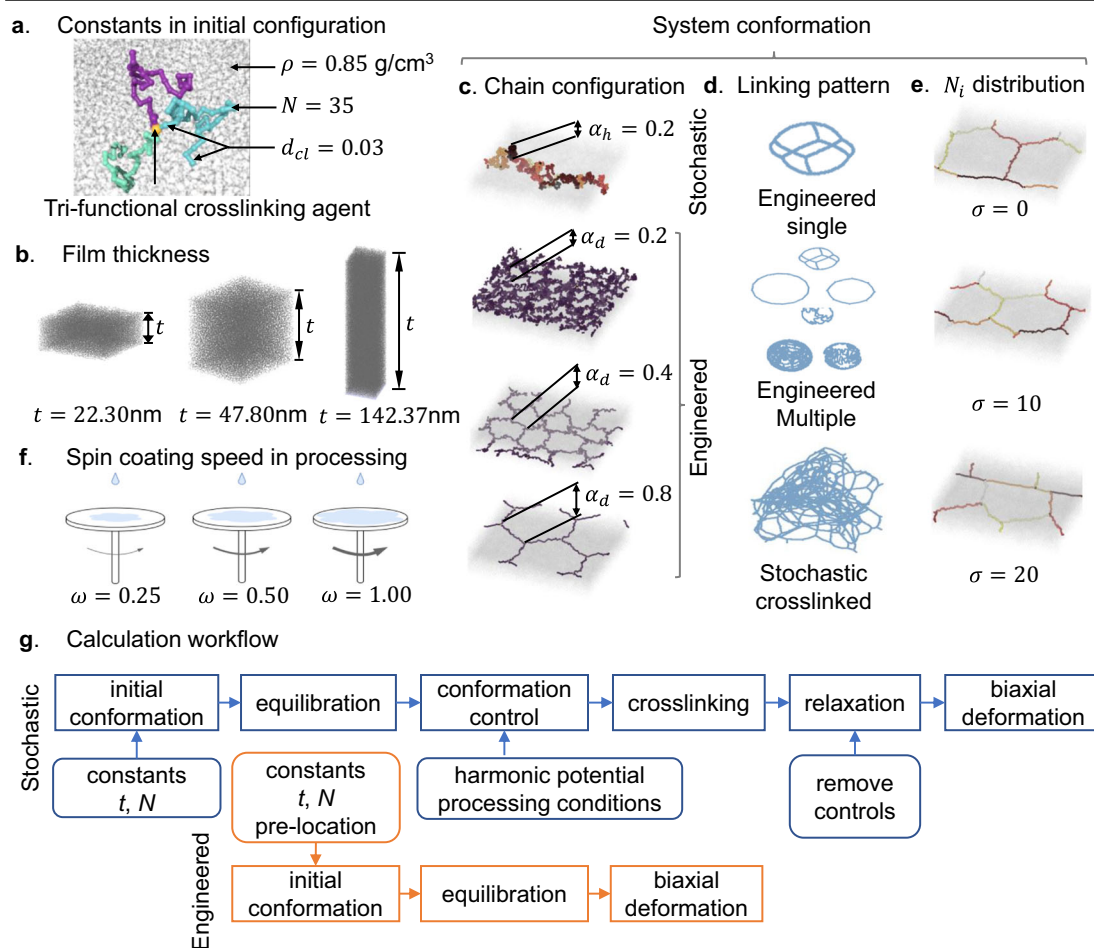
Results

CGMD polymer design framework
Crosslinked polymeric systems were constructed based on the Kremer-Grest model[33]. The molecular density and crosslinking density were kept constant (Fig. 1a) across all the polymeric systems. (see Methods, Supplementary Table 1 and Supplementary Table 2 for further information). Besides, all the chains were fully connected at both ends through tri-functional crosslinking agents (to eliminate potential stiffness enhancement simply caused by the increase of crosslink density[25], see Supplementary Fig. 1). On top of these constants, various constraints were imposed to describe a microstructural design space of the materials.

As shown in Fig. 1, our design space is composed of several key variables to systematically examine the control of conformations of the crosslinked polymers. These variables, both macroscopic and microscopic, are briefly explained as follows. Firstly, the thickness of the polymer, denoted as t, is considered for both freestanding films and those placed on substrates (Fig. 1b). Then, the end-to-end distance of individual chains (Fig. 1c), controlled by a harmonic potential added to both ends of a chain strand, is included and represented by a pre-defined uncoiling factor $\alpha = r/Nl_b$, where r is the end-to-end distance of the chain strand, N is the number of monomers between two neighboring crosslinking points, l_b is the length of CG bonds ($l_b = 1.0$). Thus, this factor α ranges from 0 (when all monomers collapse to one point) to 1 (when the chain is perfectly straight). This factor α can be controlled by either adding an external harmonic potential before crosslinking and then remove them afterward, or prelocating the crosslinkers in an orderly crosslinked polymer system (Supplementary Fig. 2), represented by α_h and α_d respectively. For the former case, the polymer chains and crosslinkers are stochastically placed in the whole simulation box and linked under the external harmonic potential α_h applied to the chains. For the latter case, the polymer chains are and crosslinkers are firstly orderly set in a plane to form layers. Then, polymer chains with same or different α_ds were stacked vertically without establishing bonds between layers to form one polymer system at a given mixing ratios while keeping the periodic boundary conditions of the polymeric simulation system. The linking pattern of the polymer network is illustrated using the graph theory with the nodes (CG beads) connected by undirected edges (CG bonds) (Fig. 1d). With this degree of freedom, distinguishment can be made between uncontrolled stochastic crosslinking (random connections of crosslinkers to mimic real synthesis operations) and engineered crosslinking patterns (ordered connections of pre-located crosslinkers theoretically synthesizable by extreme precision techniques). It should be noted that in our framework, many of the polymer systems are set to have the same N (e.g., $N = 35$). But for certain samples, the effects brought by non-uniform N are examined. As shown in Fig. 1e, this is achieved by assigning N to follow a Gaussian distribution, where its variance σ varies with a fixed mean $\mu = 35$. In addition, the processing conditions of the polymers in stochastic crosslinking can be investigated by the CGMD model, considering the variables of the film thickness t and the substrate rotating speed ω (Fig. 1f). It is worth to mention that the Kremer-Grest model we used for all the modelings and simulations of the polymer systems is a bead-spring model based on the Lennard-Jones (LJ) potential, in which the unit is not specifically fitted to a real materials system. We converted the LJ units to real units for the PDMS system, following reference by Kremer & Grest[33] (see Supplementary Table 1 for unit conversion). More detailed modeling information can be found in the Method section.

For stochastic crosslinking the polymer systems were first equilibrated adopting a two-step protocol[36], followed by conformational control, crosslinking, relaxation and biaxial in-plane tensile deformation. This whole procedure was performed three times by CGMD simulations for each case in order to obtain an

## Design and simulation of crosslinked polymers with the same crosslink density

a. Constants in initial configuration

$\rho = 0.85$ g/cm^3

$N = 35$

$d_{cl} = 0.03$

Tri-functional crosslinking agent

b. Film thickness

$t = 22.30$nm $t = 47.80$nm $t = 142.37$nm

f. Spin coating speed in processing

$\omega = 0.25$ $\omega = 0.50$ $\omega = 1.00$

System conformation

c. Chain configuration

$\alpha_h = 0.2$

$\alpha_d = 0.2$

$\alpha_d = 0.4$

$\alpha_d = 0.8$

d. Linking pattern

Engineered single

Engineered Multiple

Stochastic crosslinked

e. N_i distribution

$\sigma = 0$

$\sigma = 10$

$\sigma = 20$

g. Calculation workflow

Stochastic: initial conformation → equilibration → conformation control → crosslinking → relaxation → biaxial deformation

constants t, N

constants t, N pre-location

harmonic potential processing conditions

remove controls

Engineered: initial conformation → equilibration → biaxial deformation

Fig. 1 Schematic of the design space and controlled parameters of polymeric films in the CGMD framework. a Factors that were kept constant across all systems: molecular density ρ, number of monomers between two neighboring crosslinking points N, and crosslinking density d_{cl}. **b** Thickness of polymers in freestanding or with-substrate status: from less than the gyration of a single chain to bulk by assigning the periodic boundary condition along z direction. **c** Conformations of individual polymer chains: from uncontrolled heavily coiled chains to largely protracted chains. α is the uncoiling factor. $\alpha = r/Nl_b$, where r is the end-to-end distance of the chain strand, N is the number of monomers between two neighboring crosslinking points, l_b is the length of CG bonds ($l_b = 1.0$). α_h can be controlled by adding an external harmonic potential before crosslinking and then remove them afterward. α_d is defined by pre-locating the crosslinkers in an orderly crosslinked polymer system. **d** Crosslinking pattern represented by graph theory: stochastic crosslinking with no control, and designed crosslinking patterns with different combinations of individual chain conformations. **e** Segmental repeating unit number: from a unified number to a Gaussian distribution with different standard deviation. **f** Spin coating speed: a factor controlling the processing procedure. **g** The workflow of our simulations for stochastic crosslinked and engineered crosslinked polymer systems.

averaged tensile modulus of the polymer system. The error bars in the related figures are also obtained from the maximum and minimum value of the three runs. For engineered polymers with pre-located crosslinkers, the initial systems are crosslinked and initial conformation is already controlled. Thus, the simulation procedures are equilibration (same protocol as the first step of stochastic crosslinking) and then biaxial in-plane tensile deformation (Fig. 1g). As the pre-located crosslinkers are with no randomness, thus only the subsequent relaxation and deformation were carried out times for each case to calculate the averaged tensile modulus of the polymer system. The error bars of the related results shown in figures are likewise determined using the same approach. For all the polymeric systems, the conformational parameters were obtained after the last relaxation procedure before tensile deformation (see Method). The biaxial moduli were estimated using the data in a linear strain-stress regime, to eliminate potential ambiguities caused by nonlinear or rate-dependent behaviors (Supplementary Fig. 3).

Conformation tuned elastic moduli. In Fig. 2a, it can be seen that a pure decrease in thickness t could moderately enhance the stiffness of a polymeric system with a factor of less than 3, which may be related to a pronounced surface tension effect. However, the predicted degree of modulus increasing was far less than a maximum of around 100 times in experiments[19,37], thus, a more detailed investigation awaits to be proposed.

Leveraging the flexibility of the CGMD framework, the conformational features of the polymer system and their correlations to elastic modulus were carefully examined within thin polymeric system ($t = 22.30$ nm, r is around 5.55 nm) in Fig. 2b–e. A quasi-linear relationship of the biaxial moduli with α_h was observed in Fig. 2b. However, this aforementioned conformational perturbation method became ineffective when α_h was increased from around 0.2 (the unperturbed bulk case, see the cross mark in Fig. 2b and c, r is around 5.98 nm) to 0.4. The direct control of $\alpha_d \in (0, 0.8]$ by crosslinked initial systems pre-located crosslinkers was implemented to freely change the
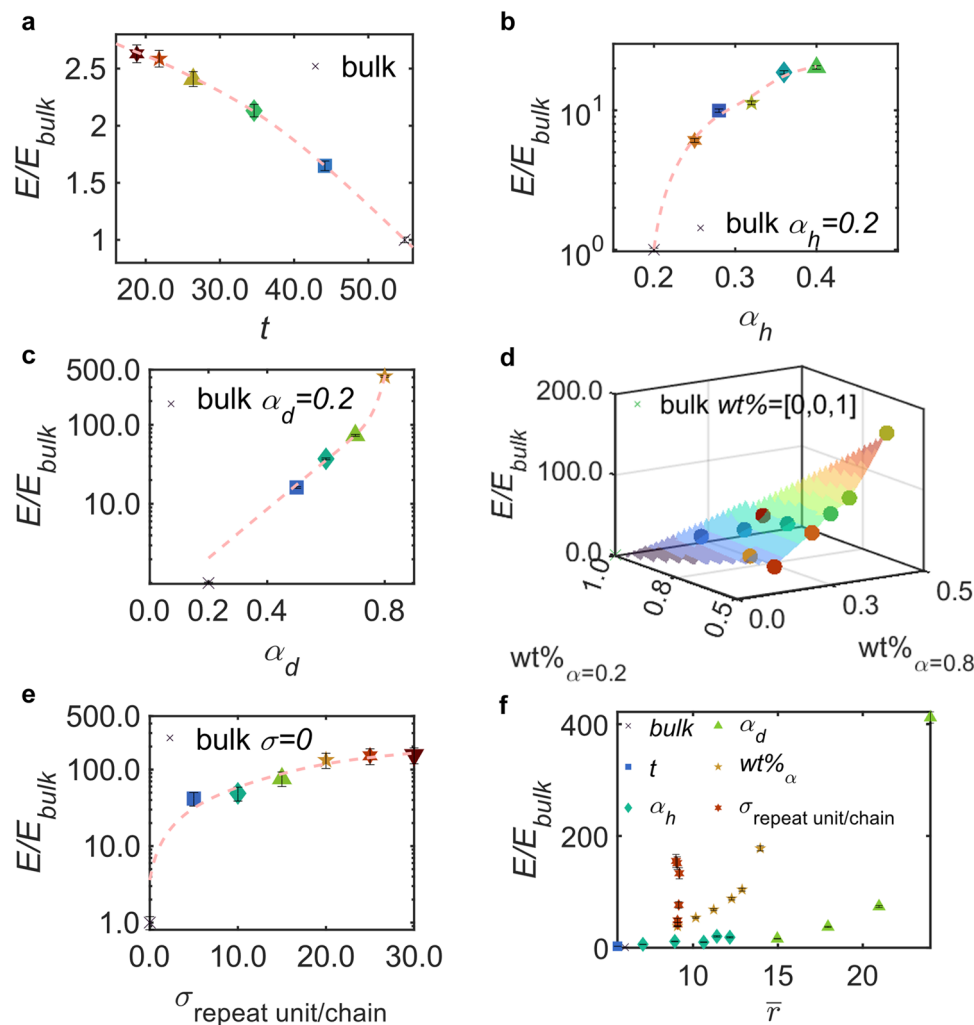
Fig. 2 Controlled paraments with bi-axial Moduli E. a Thickness t vs E. **b** Uncoiling factor α_h vs E. **c** Uncoiling factor α_d vs E. **d** Weight ratios of different pre-protracted chains with $\alpha_d = 0.2$, 0.4 and 0.8. **e** Standard deviations of the distribution of bead per chain σ vs E. **f** Mean conformational descriptor $\bar{r}$ as a sign of moduli E in each system: ✖ (dark blue cross) bulk polymer; ■ (blue square) thickness t; ◆ (light blue diamond) uncoiling factors α_h by harmonic potential; ▲ (green triangle) uncoiling factor α_d by pre-defined chain monomers and crosslinkers; ★ (yellow pentagram) weight ratio of chains with α_d combinations; ✳ (orange hexagram) randomness of monomer number per chain σ.

uncoiling factor. Interestingly, here the biaxial moduli markedly increased (by over 100 times) at a large uncoiling factor ($\alpha_d = 0.8$) (Fig. 2c). Then, a natural further step is to investigate how this stiffening effect depends on the degree of uncoiling uniformity. As shown in Fig. 2d, a two-order-of-magnitude enhancement of elastic moduli could still be achieved, with only 30% of the chains at α_d of 0.8, while the conformation of the rest 70% of the chains are at α_d of 0.2 and 0.4, similar with the conditions in bulk polymers. The non-uniformity of the distribution of N is also considered by adjusting its variance σ. In this case, the biaxial moduli show a positive relationship with σ in the range from 5 to 30 (Fig. 2e). These indicate that chains with different conformations (e.g., quantified by α) should make unequal contributions to the mechanical properties of the polymer system. Then, one interesting question could be raised: whether this conformation related stiffening behavior can be elucidated by one single descriptor via aggregating the information from all the above factors.

Scaling law. Theoretically, the mean end-to-end separation distance ($\bar{r}$) has long been considered as an important descriptor of polymer conformations, whose change could largely affect mechanical

properties of the material[38]. For example, several classic viscoelastic models, such as the Rouse model[39] and the Ngai coupling model[40], have related $\bar{r}$ to the relaxation time and the compliance of the polymer. Thus, as shown in Fig. 2f, $\bar{r}$ was estimated for each of the polymeric systems that were previously constructed in our design space with different structural parameters and processing conditions, and was then plotted against the corresponding biaxial modulus E (the mean gyration vector $\bar{G}$ against E was also tested, see Supplementary Fig. 4). While a positive correlation can be generally seen between $\bar{r}$ and E, the highly scattered data points suggest that crosslinked polymeric systems could neither be treated as ideal chains nor predicted by ideal rubbery elasticity theories. In other words, $\bar{r}$ by itself may be inadequate to serve as a descriptor, especially for the case where a drastic change in E was accompanied with nearly no change in $\bar{r}$ (the points marked by ✳).

We speculate that the inadequacy of $\bar{r}$ is due to the fact that these crosslinked polymer thin films, engineered by either direct structure designs or processing parameter controls, may result in a distribution of r significantly deviated from a Gaussian-like distribution, the one typically assumed for bulk systems. Thus, for different polymeric systems, it would be of interest to visualize the distributions of r. We use α instead of r to eliminate the variance

of N. As expected, various distinguishable features were observed on the histograms of α_i for individual chains, including drifting (Fig. 3a, b), sharpening (Fig. 3c), splitting (Fig. 3d, e) and flattening (Fig. 3f) of the peaks.

For a typical bulk elastomer system, the elastic modulus E normally scales with $3k_B T/N_{Kuhn}b^2$, where N_{Kuhn} is the number of Kuhn segment and b is the Kuhn length. Obviously, the above model can neither explain the positive relationship between E and $\bar{r}$ nor include the influence of altered r distributions. Under the same thicknesses, some of them also with same $\bar{r}$, the distribution of r could be related to the drastic change of the stiffnesses of the polymer systems. Here we
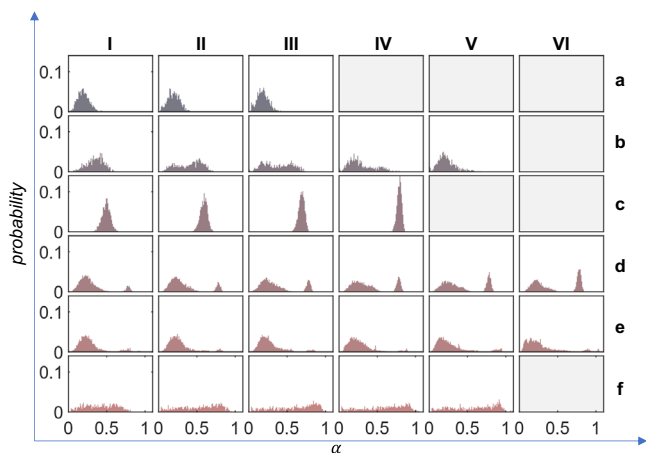

Fig. 3 The distributions of α of different polymeric systems before and after deformation. a a-I, Bulk polymer, a-II, Bulk cross-linked polymer. a-III, Thin cross-linked polymer. **b** Crosslinked polymer under uncoil harmonic potential: b-I, Peak at around 17; b-II, Peak at around 21; b-III, Peak at around 24; b-IV, Peak at around 28. (Peak shifts to the right) **c** Designed cross-linked polymer structure with a single-peak skewed distribution of α.
d Designed cross-linked polymer structure with a two-peak distribution of α: decrease of left peak height and increase of right peak height from d-I to d-VI. **e** Designed crosslinked polymer with random segmental bead number per chain shows a three-peak distribution of α. **f** Distribution of α of the polymer prepared by shear-crosslinking. The distribution is flattened by the shear in processing. The peak moves from left (f-I) to right (f-V) with the increase of shear speed.

hypothesize that in crosslinked polymeric thin film containing an amount of uncoiled chains, additional stiffening effect may need to be considered, with its magnitude positively correlated with both the number of uncoiled chains and the uncoiling degree of these chains. In the CGMD simulations, the above information can be obtained by calculating the end-to-end distance for individual chains (denoted as r_i) and counting the number of beads of chain strands i (denoted as N_i). Thus, a two-term scaling law can be proposed for explaining the simulation data and related experimental works: the first term is based on the classical model that sets the entropic contribution inversely proportional to r_i^2; while the second term accounts for a 'stiffening effect', which is expected to have a positive relationship with r_i. In addition, observed from Fig. 2, this term should be negligible for bulk systems (i.e., r_i is relatively small) and quickly rise up at some specific r_i values, exhibiting a behavior coincident with that of an activation function in artificial neural network models (e.g., a customized hyperbolic tangent function, see Supplementary Fig. 6). Thus, the relationship of the biaxial moduli and r_i can be expressed as:

$$E \cong \frac{1}{n}\left[\varphi \sum_{i=1}^{n} \frac{N_i^2}{(\bar{N}r_i)^2} + \theta \sum_{i=1}^{n}\left[1 + \tanh\left(p\frac{r_i}{N_i} - q\right)\right]\right] \quad (1)$$

where n is the total number of chain strands in the system, N_i is the number of beads (repeat units) per chain strands, $\bar{N}$ is the average number of beads per chain strand (in this case, $\bar{N} = 35$), φ and θ are the two scaling parameters tuning the stiffness of the two terms respectively, and the shape of the tanh function is controlled by the other two fitting parameters p and q. It also could be written as $E \cong \frac{1}{n}[\varphi \sum_{i=1}^{n} \frac{1}{(\bar{N}\alpha_i)^2} + \theta \sum_{i=1}^{n}[1 + \tanh(p\alpha_i - q)]]$ if we substitute r_i and N_i by α_i. When at a large enough n, the distribution of r may be approximated by a continuous probability density function $\rho(r)$. Then, the E-r relationship may be written as $E \cong \int[\varphi \frac{N_r^2}{(\bar{N}r)^2}\rho(r) + \theta(1 + \tanh(\frac{pr}{N_r} - q))\rho(r)]dr$.

The above scaling law makes consistent predictions on the CGMD simulated biaxial moduli of all the polymer configurations, while clear divergence was observed when comparing the predictions by a classical model with the CGMD data (Fig. 4a). According to the scaling result, the conventional entropic elasticity (the first term) still holds its dominating position on the elasticity for bulk polymeric system, when the uncoiling factor $\alpha = 0.2-0.3$. An increase of α, especially when α is larger than 0.7, leads to a drastic rising of the stiffening effect term (the
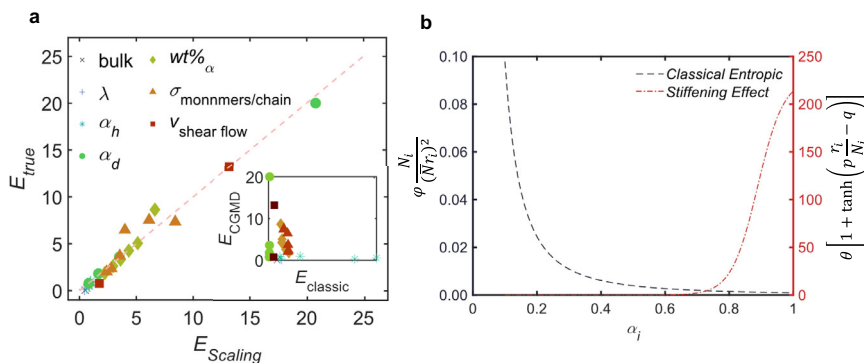
Fig. 4 Scaling results of polymeric systems. a Fitted biaxial tensile moduli versus raw CGMD data. The fitted line passes origin (0,0). The subfigure presents the results of classic entropic term versus the raw CGMD data, which cannot find clear correlations between each other. ✖ (dark blue cross) bulk polymer; + (blue plus sign) thickness t; ✳ (light blue hexagram) uncoiling factors α_h by harmonic potential; ● (green circle) uncoiling factor α_d by pre-defined chain monomers and crosslinkers; ◆ (dark green diamond) weight ratio of chains with α_d combinations; ▲ (orange triangle) randomness of monomer number per chain σ; ■ (red square) shear flow speed. **b** Decoupled the influence of the number of chains, the contribution of the conventional entropic ($\varphi \frac{N_i^2}{(\bar{N}r_i)^2}$ on the left) and the stiffening effect ($\theta[1 + \tanh(p\frac{r_i}{N_i} - q)]$ on the right) to E for individual chains with different α_is are shown (It should be noted that the intersection point of the two curves is not referential in this figure, as the left and right y axis are with different scales).

second term) with the diminishing of the first term, presumably as the major contribution to the over-two-magnitude difference between the bulk and the crosslinked polymeric nano-film (Fig. 4b).

All the examined polymer systems were well equilibrated before the biaxial tensile tests. Despite the conformational change from a bulk polymeric system, the bond distances and bond energies barely changed (e.g., <0.2% in Supplementary Table 3 and Supplementary Fig. 5). This affirms that the stiffness change of the crosslinked polymer should be mainly attributed to the alteration of chain conformations, rather than the stretching of individual chemical bonds. Certainly, the relative stiffness of the stiffening effect (that may be represented by the intersection point of the first term and second term) may depend on the crosslink density, chain length, and etc. In addition, the mechanical performance of crosslinked polymers should also be affected by their connecting modes. The moduli of a fully parallel polymer network and a perfectly series system may correspond to the upper and lower limit estimate respectively. Further demonstration of series/parallel effect of the polymer chains can be found in Supplementary Note 1, Supplementary Fig. 7 and Supplementary Equation 1. It needs to be noticed that our scaling model not solely based on theoretical deductions to explain our findings. Instead, it is a phenomenology-based function of which fitting parameters are derived from physics-based simulations.

Simulation guided thin film fabrication. Evidence has accumulated that the processing procedures, including spin coating and the cure of stochastic crosslinking (normally used to prepare crosslinked thin films like polydimethylsiloxane, i.e., PDMS), could largely change the microstructure and conformation of the polymeric system. To investigate the associated underlying mechanisms, the spin coating and polymer curing processes were simulated in our CGMD framework by applying shear velocity v_s on the substrates, effective centrifugal force f_c on the chains, and the film thickness t on the polymer microstructures (Fig. 5a, b, d–f).

When the polymer is in contact with a substrate, the simulation results showed that the applied shear velocity v_s positively correlates with r. With the increase of the spinning speed, the distribution of r becomes more flattened in contrast to a typical Gaussian distribution (Fig. 3f). According to Eq. 1, a larger r would lead to a more pronounced stiffening effect, finally causing the increase of the bi-axial modulus (Fig. 5b, c). The simulations also reveal the role that the film thickness t plays in affecting the polymer conformations. As shown in Fig. 5d, for a thick polymer film ($t = 142.37$ nm), only the chains close to the bottom substrate are stretched to a very large extent. Along the z axis, the chains in the middle section of the simulation cell are moderately affected, while the conformation of the chains in the top region almost remains unchanged (in comparison with that of a bulk system) in a statistical perspective. For the polymer film with a t of 47.80 nm, the conformations of the chains are all affected, with their degree of uncoiling descending along the z axis (Fig. 5e). However, the chains in an ultra-thin film ($t = 16.36$nm) appear to be 'stuck' to the substrate, with their conformations nearly unchanged (Fig. 5f). These phenomena suggest that a mobility gradient of the atom of the polymer chains (analogous to the concept used by Hao et al. [41]) between the adjacent layers of chains could be generated during the shearing process, which may act as the driving force for the polymer chain conformation changes. As a consequence, the elastic moduli of the system with different thickness presents a volcano-like trend (Fig. 5g). It needs to be noticed that v_s, f_c and t are correlated in real experiment processes, rather than independent with each other as we considered here. From the above discussions, the stiffening of the polymer film is a joint effect of spin coating

speed and thickness t, which clearly cannot be solely described by each single parameter. (related discussion can be found in Supplementary Fig. 7 and Supplementary Table 4).

Under the guidance of the aforementioned simulations and scaling theory, crosslinked PDMS thin films samples were prepared by a spin coating-crosslink curing procedure, using tri-functional crosslinking agent to generate connecting topologies comparable with the model. The mechanical properties of the freestanding crosslinked PDMS samples with various film thicknesses were measured on our in-house micro vibration device (Fig. 5h, see Supplementary Figs. 9 and 10). The biaxial moduli of the samples were calculated based on curvature of the photos taken by high-speed camera[19] (Fig. 5i, see Supplementary Note 2, Supplementary Eqs. 2 and 3 for calculation methods). A big increase of the biaxial modulus (~135 times) was found when the film thickness decreased from 500 nm to 50 nm (Fig. 5j), achieving a consistency among the CGMD predictions, the scaling theory and our previous experimental work[19]. This trend could be explained as follows: since thinner polymer films were fabricated by the application of a higher rotating speed, according to our model, this would lead to more stretched chains during the spin-coating process. Then, followed by an almost immediate curing process, the largely altered chain conformations were preserved from relaxation by the crosslinking. The entropic driving force of relaxation of the chain strands (chain portion between two neighboring crosslinking points) are balanced at the crosslinking points. Thus, their relaxation is prevented, resulting in the increase of the modulus. To validate this explanation, we conducted a controlled experiment wherein a 50 nm thick sample was spin-coated and allowed to undergo a 3-hour resting period at room temperature before proceeding to the heat curing stage to largely speedup the crosslinking process. In this case, while the thickness of the film did not show noticeable changes, the uncoiled chains naturally tended to recover during the 3 hours relaxation; Consequently, it was anticipated that the chain conformation in the final crosslinked film would closely resemble that of a thicker film. If our hypothesis held true, the biaxial modulus of this controlled sample should exhibit a marked decrease compared to that of the 50 nm sample that underwent immediate curing following spin coating. The stress-strain curve of the 50 nm PDMS relaxed sample was experimentally depicted by our in-house device in Fig. 5j, alongside with those of 50 nm and 500 nm PDMS films. It can be clearly observed that consistently with our expectation, polymer films with both 50 nm thickness show disparate elastic performance (with an over two-magnitude of difference) between the case of immediate crosslinking and the case of crosslinking after 3 hours relaxation. The above experiments reemphasized our findings that it is the conformational alteration of the polymers, further than nanoconfinement or thickness dependency, which induces the drastic moduli change of crosslinked polymeric thin films. In other words, in principle, a decoupling between the film thickness and film stiffness can be achieved, if the chain conformations can be independently controlled.

Discussion

This work aimed to link the elastic property of the polymeric films to the distributional information of the chain conformations, by combining a CGMD framework and experimental validations. A two-term scaling law was established to make accurate predictions on crosslinked polymer systems given a distribution of the end-to-end distances, as an important step to unveil the microscopic origin of the stiffening effect of polymer networks. Based on these findings, the investigation on the processing conditions of polymer thin films provided useful guidelines for tailoring their elastic properties for many exciting
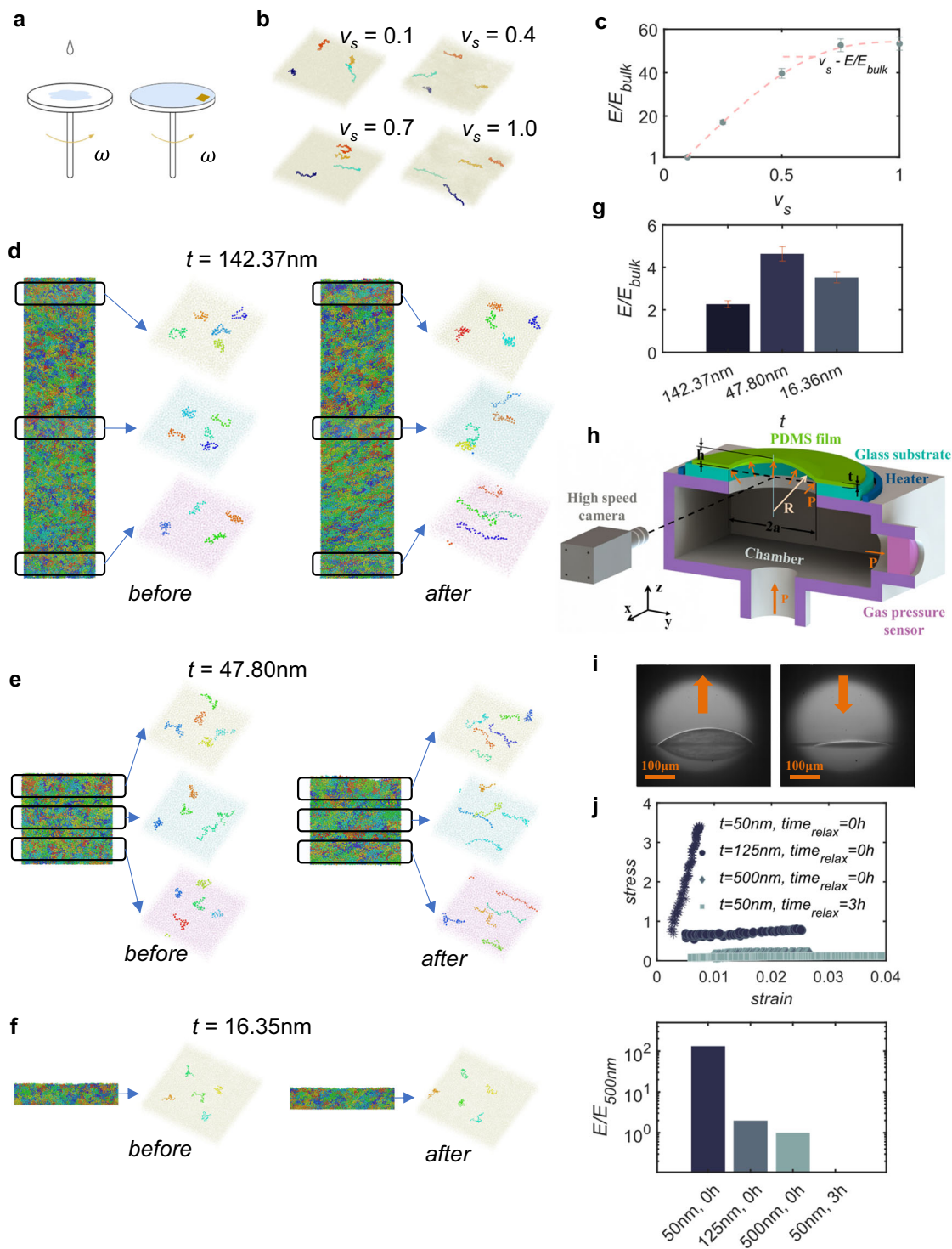
Fig. 5 Shear-crosslinking of polymer. a Schematic illustration of spin coating. Thinner films are obtained by higher spin coating speed, which also lead to confirmational changes of the polymer. The angular speed ω is converted to shear velocity v_s. **b** Conformation change under different shear velocity v_s. Higher velocity will lead to uncoiling of the chains. **c**, Relationship between shear velocity v_s and bi-axial moduli E/E_{bulk}. **d**–**f** Conformation changes at different thickness at the same spinning speed represented by the same centrifugal force f_c (The dynamics of (**b**)–(**e**) could also be found in Supplementary Fig. 8). **g** E/E_{bulk} influenced by the thickness t under same centrifugal force f_c. **h** Schematic illustration of in-house micro-vibrational test device. **i** Photo of the thin polymer films in test. **j** Experimental results of the strain-stress curve and the E/E_{500nm} to illustrate the difference in moduli between the polymer films obtained by spinning coating–relaxing(3 h)–crossing (crosslinking) and spinning coating–curing (crosslinking) without relaxation. It can be seen that after 3 h's relaxation, the Young's moduli of 50 nm polymer thin film is lower than that of the 500 nm polymer, which means that this phenomenon is more than a thickness dependency. (hexagram : $t = 50$ nm, $time_{relax} = 0$ h; circle : $t = 125$ nm, $time_{relax} = 0$ h; diamond : $t = 500$ nm, $time_{relax} = 0$ h; square : $t = 50$ nm, $time_{relax} = 3$ h.).

applications such as wearable electronics and flexible energy devices. To extend the applicability of our framework to more general polymer systems, a further step would be to develop a stable algorithm for including the factor of entanglements, which are expected to be highly correlated with the stiffness, strength, and failure of many long-chain polymers[42]. Also, while the adoption of a FENE potential in the current modeling framework is a comprise to the efficiency and flexibility of the model; for specific polymer systems, a more sophisticated potential, e.g. with the consideration of molecule anisotropy[43], may be needed for accurately describing the intermolecular and polymer-substrate interactions. Hence, the chemical species for both the polymers and the substrates may potentially be added to the parameter space, for designing better polymer films and optimizing their fabrication pathways. In addition, it may be of interest to model the breakage of chemical bonds, to enable predictions of self-healing behaviors[44,45] and/or damages of polymer networks. As a long-term goal, one promising direction is to merge the above components with the work present in this paper, to form an integrated modeling framework applicable to an even wider range of polymer systems containing both long and short chains, with or without crosslinkers. This will allow for the construction of a self-consistent and high-quality polymer database, towards a data-driven approach for engineering polymer structures with tailored mechanical properties.

Methods

Simulation basic settings. Bead-spring model extended from the Kremer and Grest model[33] was used to perform the relaxation, crosslinking and tensile test. The bonds were represented by the Finitely Extensible Nonlinear Elastic (FENE) potential while the non-bonded beads interactions were represented by 12-6 Lennard-Jones potential. The molecular density $\rho = 0.85$ g/cm^3 and the crosslinking density of 3% (see Supplementary Table 1 for conversion rule and Supplementary Table 2 for crosslinking methods in molecular simulations) were kept the same across all the polymeric systems, including both the thin film configurations and the bulk one as a reference. Crosslinked PDMS films were chosen as a representative crosslinked polymeric system, with the number of beads per chain strand N kept at 35 for all the systems (according to experiment[46] and previous simulation work[33]) except those with σs. The bond formed between crosslinkers and chain ends were considered the same with those between chain beads. All the CGMD simulations were performed via the Large-scale Atomic/Molecular Massively Parallel Simulator (LAMMPS)[47].

Conformation control and crosslinking. For simulating the stochastic crosslinking process, chains were randomly placed in the simulation box with desired molecular density (0.85 g/cm^3). To control t, simulation boxes of different thicknesses were filled by randomly positioned chains in orthogonal simulation boxes such as $t = 16.36$ nm, $t = 47.80$ nm and $t = 142.37$ nm with periodic boundary conditions on x and y directions and non-periodic boundary conditions on z direction. The density is kept the same across different thicknesses. After the creation of the initial system, equilibration was performed with a layer of atoms was created below the polymer system to represent the existence of substrate. Equilibration of the polymer film was firstly conducted with 10^4 steps under a soft dissipative particle dynamics (DPD) potential with a gradually increasing interaction force, and then 10^7 steps under a Lennard-Jones (LJ) potential for a well-established initial conformation[32,36]. After equilibration, crosslinkers are added to the system according to crosslinker density (3%). LJ walls were used to confine the polymer chains before

they are crosslinked to hold their own thin film structure. Different conformational controls were implemented as follows. To control α_h, an external harmonic potential, parametrized by the spring constant K and the equilibrium distance r_0, was added to uncoil the chains. In other cases, different velocities were added to the substrate underneath the polymers to simulate the normal speed of the substrate in processing procedures like spin coating. Or external forces were imposed to the polymer chains to simulate the radial forces created by spinning. For each of those controls, enough time was given to make it effective. Next, crosslinking bonds were created between the ends of the chains and crosslinkers. After the systems were sufficiently crosslinked, the conformational controls including walls, harmonic bonds, velocities and external forces were all removed and a further relaxation of 10^7 steps under LJ potential was done before deformation test.

For engineered polymer network patterns, crosslinkers and linking bonds were created between pre-location chains to form honeycomb-like structures (Supplementary Fig. 2) with same molecular density and crosslinker density to control α_d. The combinations of different α_ds in one polymer system were also realized by mixing engineered chain networks. For each of the pre-designed polymers, the equilibration protocol same as that used in stochastic crosslinking polymers was performed before the numerical tensile test.

Bulk polymers with a box of $x = y = z$ was simulated under full periodic boundary conditions following same equilibration-tensile test procedure for reference.

Groups with different σs from 0 to 30 linearly spaced by 5 were introduced both in stochastic crosslinking polymers and engineered polymers. The biaxial deformation tests were performed at a strain rate of 10^{-4}, and it was verified that the response of the system was not sensitive to strain rate (Supplementary Fig. 3).

The existence of substrate under the polymer system in our simulation matches the real circumstance of our experiments. In the simulation of the polymer preparation, we have a substrate below the polymer system as the polymer sample are made on a substrate by spin-coating and the subsequent curing. In the simulation of biaxial deformation under mechanical loading, substrate is not considered as we utilize an in-house vibration system to test the polymer film on which the testing parting of the polymer is freestanding in the air.

Polymer fabrication and measurement. Silicone Elastomer Kits (Sylgard® 184 purchased from Dow Corning, USA) was used to fabricate the PDMS films. A Cellulose acetate (CA) with 39.8 wt.% acetyl group (Aladdin, China) served as the sacrificial layer material to peel the film off the glass substrate. The PDMS precursors first were mixed with the crosslinking agent with a ratio of 10:1 wt./wt., then a PDMS mixture/toluene solution (4–10 wt.% solute) was spin-coated onto glass slides with rotating speeds from 2000 to 4000 rpm for 1 min. After spin-coating the sacrificial layer and the PDMS layer, the film was held at 80 °C in a vacuum oven for 5 hours. For the control experiment, the sample was relaxed at the room temperature for 3 hours before the curing step.

For the mechanical test, the stress-strain curve was obtained taking the same procedures in our previous work[19], with the equipment information and calculation formula provided by Fig. 5h, Supplementary Fig. 10, and Supplementary Eqs. 2 and 3.

Data availability
The data that support the findings of this study are available from the corresponding author upon reasonable request.

References

1. Qin, F. et al. Robust metal ion-chelated polymer interfacial layer for ultraflexible non-fullerene organic solar cells. *Nat. Commun.* **11**, 1–8 (2020).
2. Zschieschang, U., Waizmann, U., Weis, J., Borchert, J. W. & Klauk, H. Nanoscale flexible organic thin-film transistors. *Sci. Adv.* **8**, 1–11 (2022).
3. Zhao, C. et al. Layered nanocomposites by shear-flow-induced alignment of nanosheets. *Nature* **580**, 210–215 (2020).
4. Jiang, C., Markutsya, S., Pikus, Y. & Tsukruk, V. V. Freely suspended nanocomposite membranes as highly sensitive sensors. *Nat. Mater.* **3**, 721–728 (2004).
5. Xu, J. et al. Highly stretchable polymer semiconductor films through the nanoconfinement effect. *Science* **355**, 59–64 (2017).
6. Oh, J. Y. et al. Stretchable self-healable semiconducting polymer film for active-matrix strain-sensing array. *Sci. Adv.* **5**, eaav3097 (2019).
7. Sayed, S. & Selvaganapathy, P. R. High-resolution fabrication of nanopatterns by multistep iterative miniaturization of hot-embossed prestressed polymer films and constrained shrinking. *Microsyst. Nanoeng.* **8**, 20 (2022).
8. Bay, R. K., Shimomura, S., Liu, Y., Ilton, M. & Crosby, A. J. Confinement effect on strain localizations in glassy polymer films. *Macromolecules* **51**, 3647–3653 (2018).
9. Alcoutlabi, M. & McKenna, G. B. Effects of confinement on material behaviour at the nanometre size scale. *J. Phys. Condens. Matter* **17**, R461 (2005).
10. Ellison, C. J. & Torkelson, J. M. The distribution of glass-transition temperatures in nanoscopically confined glass formers. *Nat. Mater.* **2**, 695–700 (2003).
11. Li, X. & McKenna, G. B. Ultrathin polymer films: rubbery stiffening, fragility, and Tg reduction. *Macromolecules* **48**, 6329–6336 (2015).
12. O'Connell, P. A. & McKenna, G. B. Rheological measurements of the thermoviscoelastic response of ultrathin polymer films. *Science* **307**, 1760–1763 (2005).
13. VanLandingham, M. R., Villarrubia, J. S., Guthrie, W. F. & Meyers, G. F. Nanoindentation of polymers: an overview. *Macromol. Symp.* **167**, 15–44 (2001).
14. Briscoe, B. J., Fiori, L. & Pelillo, E. Nano-indentation of polymeric surfaces. *J. Phys. D. Appl. Phys.* **31**, 2395–2405 (1998).
15. Wang, G. et al. Mechanical size effect of freestanding nanoconfined polymer films. *Macromolecules* **55**, 1248–1259 (2022).
16. Stafford, C. M. et al. A buckling-based metrology for measuring the elastic moduli of polymeric thin films. *Nat. Mater.* **3**, 545–550 (2004).
17. Liu, Y. et al. Directly measuring the complete stress-strain response of ultrathin polymer films. *Macromolecules* **48**, 6534–6540 (2015).
18. Huang, J. et al. Capillary wrinkling of floating thin polymer films. *Science* **317**, 650–653 (2007).
19. Bai, P., Ma, M., Sui, L. & Guo, Y. Nanoconfinement controls mechanical properties of elastomeric thin films. *J. Phys. Chem. Lett.* **12**, 8072–8079 (2021).
20. Lee, J. H., Chung, J. Y. & Stafford, C. M. Effect of confinement on stiffness and fracture of thin amorphous polymer films. *ACS Macro Lett.* **1**, 122–126 (2012).
21. Stafford, C. M., Vogt, B. D., Harrison, C., Julthongpiput, D. & Huang, R. Elastic moduli of ultrathin amorphous polymer films. *Macromolecules* **39**, 5095–5099 (2006).
22. Saito, M., Ito, K. & Yokoyama, H. Mechanical properties of ultrathin polystyrene-b-polybutadiene-b-polystyrene block copolymer films: film thickness-dependent young's modulus. *Macromolecules* **54**, 8538–8547 (2021).
23. O'Connell, P. A., Wang, J., Ishola, T. A. & McKenna, G. B. Exceptional property changes in ultrathin films of polycarbonate: Glass temperature, rubbery stiffening, and flow. *Macromolecules* **45**, 2453–2459 (2012).
24. Yoon, H. & McKenna, G. B. 'rubbery stiffening' and rupture behavior of freely standing nanometric thin PIB films. *Macromolecules* **50**, 9821–9830 (2017).
25. Liang, H., Cao, Z., Wang, Z. & Dobrynin, A. V. Surface stress and surface tension in polymeric networks. *ACS Macro Lett.* **7**, 116–121 (2018).
26. Hanakata, P. Z., Douglas, J. F. & Starr, F. W. Interfacial mobility scale determines the scale of collective motion and relaxation rate in polymer films. *Nat. Commun.* **5**, 1–8 (2014).
27. Chang, J., Toga, K. B., Paulsen, J. D., Menon, N. & Russell, T. P. Thickness dependence of the young's modulus of polymer thin films. *Macromolecules* **51**, 6764–6770 (2018).
28. Galuska, L. A. et al. SMART transfer method to directly compare the mechanical response of water-supported and free-standing ultrathin polymeric films. *Nat. Commun.* **12**, 1–11 (2021).
29. Liu, M., Sun, J., Sun, Y., Bock, C. & Chen, Q. Thickness-dependent mechanical properties of polydimethylsiloxane membranes. *J. Micromech. Microeng.* **19**, 15–19 (2009).
30. Peng, Y., Zhang, H., Huang, X. W., Huang, J. H. & Luo, M. B. Monte Carlo simulation on the dynamics of a semi-flexible polymer in the presence of nanoparticles. *Phys. Chem. Chem. Phys.* **20**, 26333–26343 (2018).
31. Kang, J., Wang, C., Li, D., He, G. & Tan, H. Nanoscale crosslinking in thermoset polymers: a molecular dynamics study. *Phys. Chem. Chem. Phys.* **17**, 16519–16524 (2015).
32. Auhl, R., Everaers, R., Grest, G. S., Kremer, K. & Plimpton, S. J. Equilibration of long chain polymer melts in computer simulations. *J. Chem. Phys.* **119**, 12718–12728 (2003).
33. Kremer, K. & Grest, G. S. Dynamics of entangled linear polymer melts: A molecular-dynamics simulation. *J. Chem. Phys.* **92**, 5057–5086 (1990).
34. Torres, J. A., Nealey, P. F. & De Pablo, J. J. Molecular simulation of ultrathin polymeric films near the glass transition. *Phys. Rev. Lett.* **85**, 3221–3224 (2000).
35. Isaacson, S. G. et al. Fundamental limits of material toughening in molecularly confined polymers. *Nat. Mater.* **15**, 294–298 (2016).
36. Sliozberg, Y. R. & Andzelm, J. W. Fast protocol for equilibration of entangled and branched polymer chains. *Chem. Phys. Lett.* **523**, 139–143 (2012).
37. O'Connell, P. A. & McKenna, G. B. Dramatic stiffening of ultrathin polymer films in the rubbery regime. *Eur. Phys. J. E* **20**, 143–150 (2006).
38. Orr, W. J. C. Statistical treatment of polymer solutions at infinite dilution. *Trans. Faraday Soc.* **43**, 12–27 (1947).
39. Rouse, P. E. A theory of the linear viscoelastic properties of dilute solutions of coiling polymers. *J. Chem. Phys.* **21**, 1272–1280 (1953).
40. Ngai, K. L., Prevosto, D. & Grassia, L. Viscoelasticity of nanobubble-inflated ultrathin polymer films: Justification by the coupling model. *J. Polym. Sci. Part B Polym. Phys.* **51**, 214–224 (2013).
41. Hao, Z. et al. Mobility gradients yield rubbery surfaces on top of polymer glasses. *Nature* **596**, 372–376 (2021).
42. Kim, J., Zhang, G., Shi, M. & Suo, Z. Fracture, fatigue, and friction of polymers in which entanglements greatly outnumber cross-links. *Science* **374**, 212–216 (2021).
43. Everaers, R. & Ejtehadi, M. R. Interaction potentials for soft and hard ellipsoids. *Phys. Rev. E - Stat. Phys., Plasmas, Fluids, Relat. Interdisc. Top.* **67**, 8 (2003).
44. Li, C. H. et al. A highly stretchable autonomous self-healing elastomer. *Nat. Chem.* **8**, 618–624 (2016).
45. Rao, Y. L. et al. Stretchable self-healing polymeric dielectrics cross-linked through metal-ligand coordination. *J. Am. Chem. Soc.* **138**, 6020–6027 (2016).
46. Hwang, J. et al. Unveiling viscoelastic response of capacitive-type pressure sensor by controlling cross-linking density and surface structure of elastomer. *ACS Appl. Polym. Mater.* **2**, 2190–2198 (2020).
47. Thompson, A. P. et al. LAMMPS - a flexible simulation tool for particle-based materials modeling at the atomic, meso, and continuum scales. *Comput. Phys. Commun.* **271**, 108171 (2022).

Author contributions

Yanming Wang and Yunlong Guo conceptualized and supervised the project. Zhengyang Zhang performed the numerical calculation. Pei Bai and Yuhan Xiao conducted the experiment. Zhengyang Zhang and Pei Bai wrote the manuscript. Everyone participated in the results analysis, discussions and the revisions of the manuscript.

Competing interests

The authors declare no competing interests.

Additional information

Supplementary information The online version contains supplementary material available at https://doi.org/10.1038/s42005-023-01450-3.

Correspondence and requests for materials should be addressed to Yunlong Guo or Yanming Wang.

Peer review information *Communications Physics* thanks the anonymous reviewers for their contribution to the peer review of this work.

Reprints and permission information is available at http://www.nature.com/reprints

Publisher's note Springer Nature remains neutral with regard to jurisdictional claims in published maps and institutional affiliations.